

# Experimental demonstration of a DSP-based cross-channel interference cancellation technique for application in digital filter multiple access PONs

Giddings, Roger; Al-Rawachy, Ehab; Tang, Jianming

**Optics Express**

*DOI:*
10.1364/OE.25.003850

Published: 14/02/2017

Peer reviewed version

# Experimental demonstration of a DSP-based Cross-Channel Interference Cancellation technique for application in Digital Filter Multiple Access PONs

**E. AL-RAWACHY[1,2], R.P. GIDDINGS[1,*] AND J.M. TANG[1]**

*1. School of Electronic Engineering, Bangor University, Dean Street, Bangor, LL57 1UT, UK*
*2. College of Electronics Engineering, Electronics department, Ninevah University, Mosul, Iraq*
[*] *r.p.giddings@bangor.ac.uk*

**Abstract:** A DSP-based cross-channel interference cancellation (CCIC) technique with initial condition-free, fast convergence and signal modulation format independence, is experimentally demonstrated in a two-channel point-to-point digital filter multiple access (DFMA) PON system based on intensity-modulation and direct-detection (IMDD). The CCIC-induced transmission performance improvements under various system conditions are fully investigated for the first time. It is shown that with one iteration only the CCIC technique can achieve a reduction in individual OFDM subcarrier BERs of more than 1000 times, an increase in transmission capacity by as much as 19 times and an increase in optical power budget by as much as 3.5dB. The CCIC technique thus has the potential to drastically improve the transmission performance of DFMA PONs.

## References and links

1. Cisco Global Cloud Index: Forecast and Methodology, 2015–2020 White Paper. http://www.cisco.com/c/dam/en/us/solutions/collateral/service-provider/global-cloud-index-gci/white-paper-c11-738085.pdf
2. TV and Media 2015. The empowered TV and media consumer's influence. An Ericsson Consumer Insight Report (2015) https://www.ericsson.com/res/docs/2015/consumerlab/ericsson-consumerlab-tv-media-2015.pdf
3. Bell Labs Consulting, Nokia, "Who will satisfy the desire to consume? How will wireless data demand grow between now and 2020 and how should mobile operators respond? ",https://pages.nokia.com/1503.bell-labs-mobility-report.html?gseu
4. J. E. Mitchell, "Integrated wireless backhaul over optical access networks," J. Lightwave Technol., **32**(20), 3373-3382 (2014).
5. N. Zilberman, P. M. Watts, C. Rotsos and A. W. Moore, "Reconfigurable Network Systems and Software-Defined Networking", in Proceedings of the IEEE, **103**(7), 1102-1124, (2015).
6. M. Bolea, R. P. Giddings, and J. M. Tang, "Digital orthogonal filter enabled optical OFDM channel multiplexing for software-reconfigurable elastic PONs," J. Lightwave Technol., **32**(6), 1200–1206, (2014).
7. M. Bolea, R. P. Giddings, M. Bouich, C. Aupetit-Berthelemot, and J. M. Tang, "Digital filter multiple access PONs with DSP-enabled software reconfigurability," J. Opt. Commum. Netw., **7**(4), 215-222, (2015).
8. X. Duan, R. P. Giddings, M. Bolea, Y. Ling, B. Cao, S. Mansoor, and J. M. Tang, "Real-time experimental demonstrations of software reconfigurable optical OFDM transceivers utilizing DSP-based digital orthogonal filters for SDN PONs," Opt. Express, **22**(16), 19674-19685, (2014).
9. W. Jin, X. Duan, Y. Dong, B. Cao, R. P. Giddings, C. F. Zhang, K. Qiu, and J. M. Tang, "DSP-enabled flexible ROADMs without optical filters and O-E-O conversions," J. Lightwave Technol., **33**(19), 4124-4131, (2015).
10. L. Tao, Y. Wang, Y. Gao, A. Pak Tao Lau, N. Chi, and C. Lu, "40 Gb/s CAP32 System With DD-LMS Equalizer for Short Reach Optical Transmissions," IEEE Photon. Technol. Lett., **25**(23), 2346-2349, (2013).
11. A.L.C. Hui et. al., "Successive Interference Cancellation for Multiuser Asynchronous DS/CDMA Detectors in Multipath Fading Links", IEEE Tran. Comm, 46(3), 384-391,(1998).
12. Y. Dong, E. Al-Rawachy, R. P. Giddings, W. Jin, D. Nesset, and J. M. Tang, "Multiple Channel Interference Cancellation of Digital Filter Multiple Access PONs," J. Lightwave Technol., Early Access Article (2016).

## 1. Introduction

There are many recently emerging trends significantly impacting internet data traffic, such as the advent of cloud-based computing services [1], the sharp growth in user generated content, the rapidly increasing consumption of on-demand video-centric services [2] and the explosive growth in smart mobile devices [3]. There is also the growing traffic generated by the machine-to-machine (M2M) and Internet of Things (IoT) industry segments which have relatively low impact on data traffic but more significant implications for signaling traffic [3]. These various trends are driving both system/equipment vendors and network operators to reexamine traditional network architectures, as current networks tend to support predominantly static traffic patterns with predefined physical connections providing end users with dedicated bit rates having limited flexibility. However, such a static service provision approach is ill-suited to the dynamic, reconfigurable and elastic interconnect needs of today's emerging digital services. Furthermore, to achieve sustainable and economically viable future network solutions, which can adapt and scale to meet highly dynamic future network demands, the seamless convergence of traditional access networks, metro networks and 4G/5G mobile front-haul/back-haul networks [4] into a dynamically reconfigurable cloud access network (CAN) complemented with the software defined networking (SDN) [5] paradigm is also becoming an essential network development strategy.

To provide highly desirable dynamic software-reconfigurable networking in a cloud access network scenario down to the physical layer, we have recently proposed a new multiple access technique termed digital filter multiple access (DFMA), which is applicable to both CANs and conventional passive optical networks (PONs). The DFMA technique uses the power of optical transceiver-embedded digital signal processing (DSP) to realise SDN controlled on-line channel multiplexing/demultiplexing to allow multiple users and/or services to dynamically share a common fibre transmission medium [6-8]. The DFMA technique enables optical transceivers to support reconfigurable and elastic connections which can be dynamically configured by a centralised SDN controller according to the transient network requirements. Furthermore, when combined with optical filter- and E-O-E conversion-free, reconfigurable optical add/drop multiplexers (ROADMs) [9] that perform DFMA channel add/drop operations at the wavelength, sub-wavelength and orthogonal sub-band levels, the DFMA technique can also enable highly flexible network architectures that exploit rapid traffic-dependent reconfiguration to efficiently utilise network resources.

The performance characteristics of multipoint-to-point intensity-modulation and direct-detection (IMDD)-based DFMA-PONs have been numerically investigated [7] for scenarios with up to 32 DFMA channels each carrying OFDM modulated signals, the ONU count-dependency of maximum signal transmission capacity and system power budget have also been fully explored. Additionally the filter design-dependent system performance trade-offs have also been investigated to determine optimum filter parameters for various scenarios. Furthermore, a two-channel real-time OFDM-based IMDD point-to-point DFMA-PON system has also been experimentally demonstrated over a 25km SSMF link [8]. The real-time point-to-point DFMA-PON demonstration [8] has clearly revealed that its system performance is highly reliant on the preservation of spectrally-overlapped channel orthogonality which can be dependent on effects such as component and channel frequency responses as well as the nonlinearities mainly associated with optical signal transmission.

It is easy to understand that cross-channel interference (CCI) occurs when channel orthogonality is not perfect, and the CCI level increases as the level of channel orthogonality decreases, the CCI effect thus leads to reduced system performance due to the unwanted signal leakage from one channel to its corresponding orthogonal channel. Real-time point-to-point

electrical back-to-back DFMA-PON experiments, which eliminate all nonlinear optical effects but still maintain significant channel frequency response roll-off-induced linear CCI, have still exhibited a significant reduction in system performance. This has been verified by comparing the channel performance with the corresponding orthogonal channel enabled and disabled, the channel frequency response-induced linear CCI results in clear signal leakage between channels, mainly in the spectral region corresponding to the lower frequency OFDM subcarriers [8].

To mitigate the CCI induced by linear and nonlinear effects, two previously published DSP-based techniques can potentially be applied, which include least mean square (LMS)-based equalization [10] and successive interference cancellation (SIC) [11]. The LMS-based equalization has the disadvantages of: i) a large number of iterations can be required to achieve the performance convergence, which contributes to an increase in the total switching delay during network reconfiguration ii) high convergence sensitivity to initial conditions, which means convergence cannot always be guaranteed, and iii) the optimum tap count and step size can also be system-dependent [10]. Other drawbacks of LMS-type algorithms are also discussed in [12]. On the other hand, to receive a strong signal in the presence of a weaker signal, the SIC technique typically involves complicated DSP procedures including: i) the full bit-level decoding of the stronger signal, ii) the reconstruction of the modulated signal and its subtraction from the combined received signal, and finally iii) the extraction of the weaker signal from the residual signal. Successive iterations are, subsequently, applied to attain the required performance. It may be possible to adapt and apply the SIC technique to address the CCI problem, however the need to fully decode the signal to the bit-level and reconstruct the modulated signal results in the following three disadvantages: i) implementation dependence on signal modulation format, ii) very high DSP complexity, which would be especially high for the case of OFDM modulation, and iii) unacceptably high latency.

To effectively mitigate the CCI effect using a low DSP-complexity approach for any DFMA-based transmission system, we have proposed and experimentally demonstrated a simple but highly effective DSP-based CCI cancellation (CCIC) technique [13], which operates by estimating and subsequently cancelling the CCI signals associated with IMDD point-to-point DFMA-PON systems. The proposed CCIC technique is modulation format-independent, has comparatively low DSP complexity, requires only a single CCIC iteration and it is completely free from dependence on any initial conditions. In this paper we perform in-depth experimental investigations of the CCIC-induced system performance improvements in a digital orthogonal filter multiplexed point-to-point DFMA-PON system employing two IMDD OFDM signals. We investigate improvements in terms of individual OFDM subcarrier bit error rates (BERs), total signal transmission capacity and optical power budget. The results presented in this paper demonstrate that the CCIC technique can lead to substantial performance improvements when applied to IMDD DFMA PONs.

## 2. Digital Filter Multiple Access PONs

The DFMA technique employs channel multiplexing operations fully implemented by DSP functions in the digital domain, thus no additional analogue electrical or optical components are required, compared to conventional PONs. Employing purely integrated circuit (IC)-based DSP implies that the technique can be highly cost effective due to the inherent low cost of mass produced digital ICs.

Figure 1 shows a simplified top level architecture of a DFMA-PON system [7]. Only the upstream direction is shown in Fig.1, however the downstream direction employs the same fundamental operating principle. In a DFMA-PON, transceiver-embedded digital filters allow the provision of N independent channels by dividing the available electrical signal bandwidth of $B$ Hz into a set of $N/2$ sub-bands with equal bandwidth of $B_{SUB} = 2B/N$ Hz. Each sub-band consisting of spectrally-overlapped orthogonal in-phase and quadrature-phase channels. In the digital domain, finite impulse response (FIR)-based digital orthogonal filters are combined with

signal up-sampling (down-sampling) to multiplex (demultiplex) a signal to (from) any of the available DFMA channels within the full set of $N$ available channels. Each individual transceiver can also support multiple channels by implementing multiple FIR filter instances in parallel. A transceiver can also be readily designed to support an elastic channel bandwidth, where the orthogonal sub-band bandwidth is $B_{SUB} \cdot 2^k$ Hz, were k=0, 1, 2, . . , $\text{Log}_2(N/2)$. The DFMA channel allocation is dynamically reconfigurable by reprogramming the FIR filter coefficients to select the suitable filter frequency response corresponding to the traffic requirement, the programming of the FIR coefficients would be performed under the control of a transceiver-embedded DSP controller which periodically communicates with the centralized SDN network controller [7].

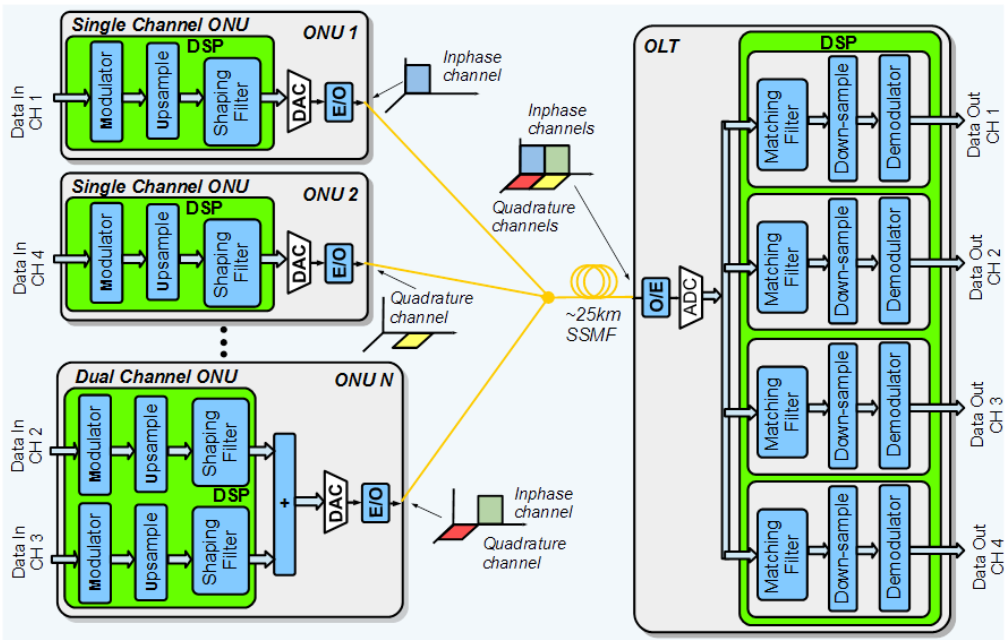


Fig. 1. DFMA-PON top level architecture

To multiplex two orthogonal channels within the same spectrally-overlapped sub-band, two digital filters are used which form a Hilbert-pair and have the same central frequency and nominal bandwidth as the targeted DFMA sub-band. The impulse responses for the transmitter-side Hilbert-pair shaping filters for the $i$th sub-band are represented as $s_i^I(t)$ for the in-phase filter and $s_i^Q(t)$ for the quadrature-phase filter. The characterisation of the Hilbert-pair transmit filters has been fully defined in [7]. The corresponding impulse responses for the receiver-side Hilbert-pair matching filters for the $i$th sub-band, are $m_i^I(t)$ and $m_i^Q(t)$ where:

$$\begin{aligned} m_i^I(t) &= s_i^I(-t) \\ m_i^Q(t) &= s_i^Q(-t) \end{aligned} \tag{1}$$

For simplicity, in this paper, a point-to-point DFMA PON system conveying two channels orthogonally occupying the same spectral region is considered, as shown in Fig. 2, thus for this case $i$=1. The Hilbert pair-based digital filters combined with up-sampling/down-sampling functions achieve orthogonality between these two sub-band channels such that:

$$s_1^A(t) \otimes m_1^B(t) = \begin{cases} \delta(t - T_0), & A = B \\ 0 \quad , & A \neq B \end{cases} \tag{2}$$

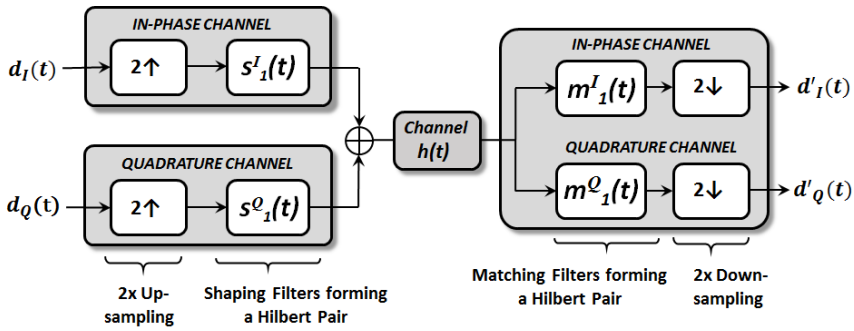


Fig. 2. Two channel digital filter multiplexing using Hilbert pair-based filters

where the superscripts *A* and *B* each denote *I* or *Q* and $T_0$ corresponds to the fixed time delay induced by the digital filtering process. Thus if the inputs to the in-phase channel and quadrature-phase channel are $d_I(t)$ and $d_Q(t)$ respectively and there is an ideal, zero loss and zero delay channel from the shaping filter outputs to the matched filter inputs, the output signal $d'_I(t)$ from the in-phase matched filter is:

$$d'_I(t) = [d_I(t) \otimes s_1^I(t) \otimes m_1^I(t)] + [d_Q(t) \otimes s_1^Q(t) \otimes m_1^I(t)] \tag{3}$$

Using the orthogonality property of the Hilbert-pair filters defined in Eq. (2), the first convolution term in Eq. (3) becomes a delayed version of $d_I(t)$ and the second term becomes zero, thus:

$$d'_I(t) = [d_I(t) \otimes \delta(t - T_{CH})] \tag{4}$$

here $T_{CH}$ is included to represent the total system propagation delay between the transmitter's shaping filter input to the receiver's matching filter output. Similarly, the output signal from the quadrature-phase matched filter in the receiver is a delayed version of the input signal at the quadrature-phase shaping filter in the transmitter, thus:

$$d'_Q(t) = [d_Q(t) \otimes \delta(t - T_{CH})] \tag{5}$$

Thus for the ideal channel case and with ideal filter responses, perfect orthogonality between the spectrally-overlapped orthogonal channels is maintained and the digital filter multiplexing and demultiplexing operations do not introduce any CCI between these two channels. The practical FIR digital filters employed provide an approximation to the ideal, infinitely long, Hilbert-pair filter impulse responses, however the filter lengths can be suitably truncated to practical lengths as demonstrated in [6, 7].

## 3. Cross-Channel Interference and Cancellation Principle

### *3.1 Cross-Channel Interference*

In section 2 the case of an ideal, zero loss channel is considered, however in a real transmission system, the overall channel frequency response between the transmit-side and receive-side DFMA filters typically exhibits a frequency response roll-off characteristic, where the channel attenuation increases with frequency. In a point-to-point IMDD DFMA PON system employing DSP-based channel reconfigurable optical transceivers, the frequency response roll-off effect is mainly attributed to: i) the sin(x)/x response associated with zero-order-hold digital-to-analogue converters (DACs), ii) the low-pass response of the DAC/ADC analogue front-ends, and iii) the frequency selective channel fading effect associated with the IMDD transmission system. If *h(t)* represents the overall channel impulse response of the complete physical channel between the shaping filter output in the transmitter and the matching filter input in the receiver, the signal output from the in-phase matching filter, $d'_I(t)$ is now:

$$d'_I(t) = [d_I(t) \otimes s_1^I(t) \otimes h(t) \otimes m_1^I(t)] + [d_Q(t) \otimes s_1^Q(t) \otimes h(t) \otimes m_1^I(t)] + w_I(t) \quad (6)$$

The first term on the right of Eq. (6) reflects the wanted signal $d_I(t)$ which is however subject to the effect of *h(t)*. The second term on the right is now non-zero and so the output of the in-phase matched filter also contains a component dependent on $d_Q(t)$, thus the received signal on the in-phase channel consists of a wanted component originating from the in-phase channel and an unwanted CCI component originating from the quadrature-phase channel. $w_I(t)$ represents the received noise component on the in-phase channel due to all noise sources in the transmission system. It can be shown in a similar manner that there exists CCI from the in-phase channel to the quadrature-phase channel, thus:

$$d'_Q(t) = [d_Q(t) \otimes s_1^Q(t) \otimes h(t) \otimes m_1^Q(t)] + [d_I(t) \otimes s_1^I(t) \otimes h(t) \otimes m_1^Q(t)] + w_Q(t) \quad (7)$$

where $w_Q(t)$ represents the received noise component on the quadrature-phase channel due to all noise sources in the transmission system. The unwanted CCI components generated between orthogonal channels can result in a severe degradation of the transmission performance of both channels, therefore it is highly advantageous if a simple and highly effective transceiver-embedded DSP algorithm can be exploited to mitigate the effect of the CCI.

### *3.2 Cross-Channel Interference Cancellation Principle*

The interference signal, $c_{QI}(t)$ from the quadrature-phase channel to the in-phase channel as determined in Eq. (6) is:

$$c_{QI}(t) = d_Q(t) \otimes s_1^Q(t) \otimes h(t) \otimes m_1^I(t) \quad (8)$$

It is shown in Eq. (8) that, in order to ideally reconstruct the interference signal at the receiver, the transmitted signal $d_Q(t)$ must be known at the receiver. However as $d_Q(t)$ is obviously unavailable, the actual received signal on the quadrature-phase channel, $d'_Q(t)$, can be used as an estimate as it closely approximates to a scaled version of $d_Q(t)$. Thus as the shaping and matching filter responses are known and as the channel impulse response can be easily determined by a training sequence-based, channel estimation DSP function in the receiver, an estimate of the interference signal, $e_{QI}(t)$, can be generated as follows:

$$e_{QI}(t) = [d'_Q(t) / S_Q] \otimes s_1^Q(t) \otimes h(t) \otimes m_1^I(t) \quad (9)$$

where $S_Q$ represents the scaling factor of $d'_Q(t)$, relative to $d_Q(t)$. Thus to generate $e_{QI}(t)$ it is clear from Eq. (9) that a 3-stage DSP filter process is required, which corresponds to convolution by $s_1^Q(t)$, $h(t)$ and $m_1^I(t)$, with scaling by $S_Q^{-1}$. It is also necessary to apply 2×up-sampling (2×down-sampling) before (after) the filtering and scaling functions to replicate the exact signal path that generates the CCI effect. A similar approach can be used to estimate the interference signal, $e_{IO}(t)$, from the in-phase channel to the quadrature-phase channel. The

generated CCI signal estimates are then subtracted from suitably delayed versions of the received signals on each channel to cancel out the CCI, thus;

$$d_I''(t) = d_I'(t - T_E) - e_{QI}(t),$$
$$d_Q''(t) = d_Q'(t - T_E) - e_{IQ}(t) \quad (10)$$

where $d''_I(t)$ [$d''_Q(t)$], is the new received signal estimate for the in-phase channel [quadrature-channel] and $T_E$ is the delay of the interference estimation function. $T_E$ is therefore the delay which is applied to the received signals to align the actual and estimated interference signals. The resultant received signals are then passed to the appropriate demodulation functions for data recovery. The value of $T_E$ can be determined from the knowledge of the estimate of $h(t)$ and the corresponding shaping and matching filters in the interference estimation function. If the CCIC function does not completely remove the CCI component in the received signal and as the resultant signals are improved estimates of the transmitted signals, the new received signal estimates could then be applied to a second CCIC iteration stage which could in theory further reduce any remaining CCI signal components. It is feasible that multiple CCIC iterations may be beneficial, however the need for multiple iterations will naturally be dependent on the accuracy of the CCI signal estimates.

Our numerical simulations have indicated that the transmission performance of a channel allocated at a specific sub-band is dominantly affected by the CCI caused by its orthogonal counterpart occupying the same sub-band, and that the impacts of all other channels simultaneously occupying other sub-bands are negligible. This implies that the above-described CCIC technique is applicable for any downstream and upstream DFMA-PON systems accommodating multiple sub-bands.

As an example of the practical implementation of the CCIC technique, the top level DSP architecture of a two-channel point-to-point DFMA PON system employing OFDM modulated signals is shown in Fig. 3 and Fig.4, the location of the CCIC DSP block is clearly shown in the receiver side DSP. In the following description, the in-phase (quadrature-phase) channel is referred to as channel 1 (channel 2). The detailed internal functions of the CCIC block are detailed in Fig. 4(a) which consists of two CCIC stages to allow the impact of a second CCIC iteration to be explored. Within each CCIC stage there are two interference estimation functions, one function estimates the interference from channel 1 to channel 2 and the second function estimates the interference from channel 2 to channel 1. Within each CCIC stage the incoming signals are suitably delayed before the estimated interference signals are subtracted. The output signals from CCIC stage 1 then pass to the CCIC stage 2 where the same process is repeated. Fig. 4(b) shows the internal operations of the interference estimation functions, which consist of the aforementioned up-sampling/down-sampling, filtering and scaling operations.

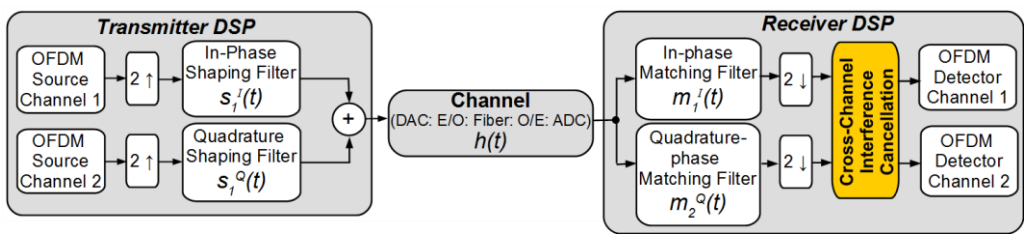


Fig. 3. Top level DSP architecture of a 2-channel point-to-point DFMA system carrying OFDM signals on each channel.

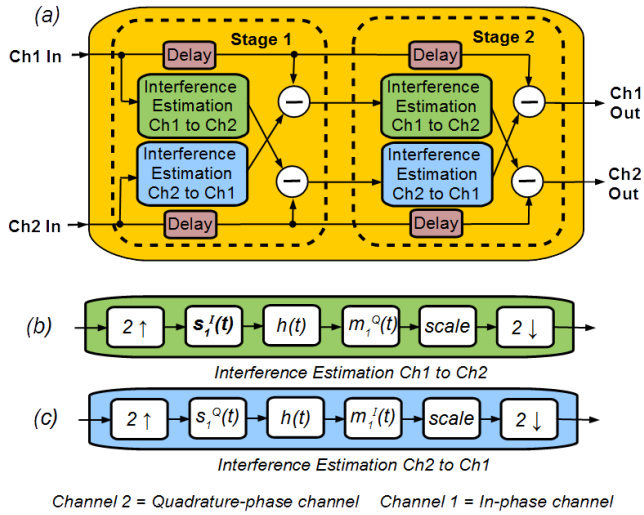


Fig. 4. (a) 2 stage Cross-Channel Interference Cancellation function. Interference estimation functions: (b) Channel 1 to Channel 2 and (c) Channel 2 to Channel 1

## 4. Experimental System Setup

Figure 5 shows the considered point-to-point DFMA-PON experimental system setup with key system parameters listed in Table 1. A field programmable gate array (FPGA)-based real-time transmitter with an 8-bit DAC operating at 2GS/s is employed to generate and multiplex via digital filtering two orthogonal DFMA channels. An RF gain stage sets the optimum RF signal voltage at 2.2Vpp for combination, via a bias-T, with an optimum DC bias of −0.7V. The resultant RF signal intensity modulates a 10GHz electro-absorption modulator (EAM) within an EML. The 1550nm DFB laser in the EML is driven with a 125mA bias current. The EML's optical output is launched at an optical power of 2dBm into varying lengths of an SMF IMDD system.

At the receiver, the received optical signal passes through a variable optical attenuator (VOA) to control the received optical power (ROP) level, optical-electrical conversion is then performed by a 12.4GHz photodetector with integrated transimpedance amplifier, this is followed by a RF gain stage and a low pass filter to optimize the electrical signal level fed into a digital storage oscilloscope (DSO). The DSO samples the signal at 25GS/s and then performs off-line DSP using MATLAB™. The off-line DSP function first resamples the signal to 26GS/s before down-sampling to 2GS/s to match the transmitter sample rate. As the absolute sample timing offset (STO) of the sampling instances in the receiver is critical for maintaining channel orthogonality, the off-line DSP determines the optimum STO when down-sampling from 26GS/s to 2GS/s. By varying the sample offset when down-sampling the STO can be changed in increments of 38.46ps, due to the two times up-sampling it is necessary to sweep the STO across two sample periods at 2GS/s (1ns). The total BER for the in-phase channel is computed for the 26 possible STO values to identify the optimum STO for use with the remaining receiver DSP functions. The subsequent off-line DSP functions performed are as follows: in-phase and quadrature-phase match filtering, two times down-sampling, CCIC signal processing according to the principle described in section 3.2 and OFDM signal demodulation for each of the two received signals.

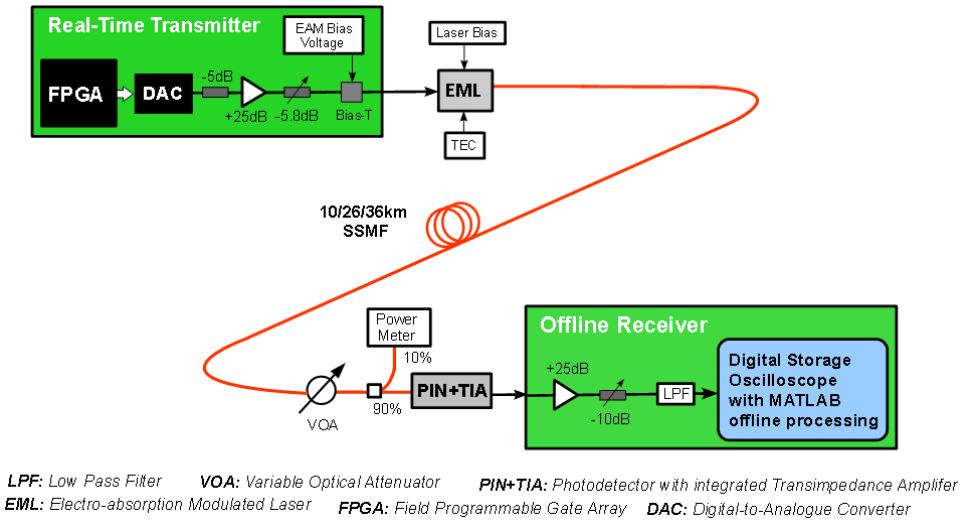


Fig. 5. Point-to-point two-channel DFMA-PON experimental system setup.

**Table 1. Transceiver and system parameters**

| Parameter | Value |
|---|---|
| Total number of IFFT/FFT points per channel | 32 |
| Maximum data-carrying subcarriers per channel | 15 |
| n-th subcarrier frequency | n×31.25MHz |
| Modulation formats on all subcarriers | 16-QAM |
| DAC sample rate | 2GS/s |
| DAC resolution | 8 bits |
| Oscilloscope sample rate [re-sampled rate] | 25GS/s [2GS/s] |
| OFDM symbol rate | 25MHz # |
| Samples per symbol (IFFT) | 32 samples (32ns) # |
| Cyclic prefix | 8 samples (8ns) # |
| Total samples per symbol | 40 samples (40ns) # |
| EML laser wavelength | 1550nm |
| 3-dB EML modulation bandwidth | 10GHz |
| Laser bias current | 125mA |
| EAM bias voltage | -0.7V |
| EML driving voltage | 2.2Vpp |
| PIN detector bandwidth | 12.4GHz |
| PIN detector sensitivity | -19dBm* |
| System frequency response roll-off (signal spectral region) | 10.5dB |

# Before up-sampling and after down-sampling
* Corresponding to 10 Gb/s non-return-to-zero data at a BER of $1.0 \times 10^{-9}$

## 5. Experimental results

### *5.1 Channel Frequency Response and Impulse Response*

Figure 6 shows the normalised amplitude and phase profiles of the channel frequency response *H(f)* of the complete physical point-to-point IMDD DFMA-PON system between the digital domains in the transmitter and the receiver. The complete system consists of the transmitter side elements comprising a DAC, a RF gain stage and an EML intensity modulator, the 26km SMF optical link, as well as the receiver side elements comprising a variable optical attenuator,

a PIN photodetector, a RF gain stage and a DSO-embedded ADC. The system frequency response is measured with a conventional optical OFDM system at the 15 discrete OFDM subcarrier frequencies spaced at 62.5MHz (with no digital filtering or up/down-sampling, the conventional OFDM subcarrier frequencies are twice that of the DFMA system). As expected, Fig. 6(a) and Fig. 6(b) show that the overall frequency response roll-off across the 0-1GHz spectral region is 10.5dB, and that the phase profile has an almost linear developing trend across the same signal spectral region.

For the results in this section obtained using the CCIC technique, the required discrete system impulse response *h(t)* is determined by performing a 32 point inverse fast Fourier transform (IFFT) on the doubled sided spectrum of *H(f)*. The fact that *H(f)* is normalised to the gain at the first subcarrier frequency is simply compensated for by an adjustment to the linear scaling factor used in the interference estimation function. As the frequency selective channel fading effect associated with the IMDD dispersive system is just one of several factors contributing to the total system frequency response roll-off effect, *H(f)* does not vary significantly for the different lengths of SMF employed in the measurements, therefore the discrete system impulse response *h(t)* determined at 26km SMF is also used for all fiber lengths.

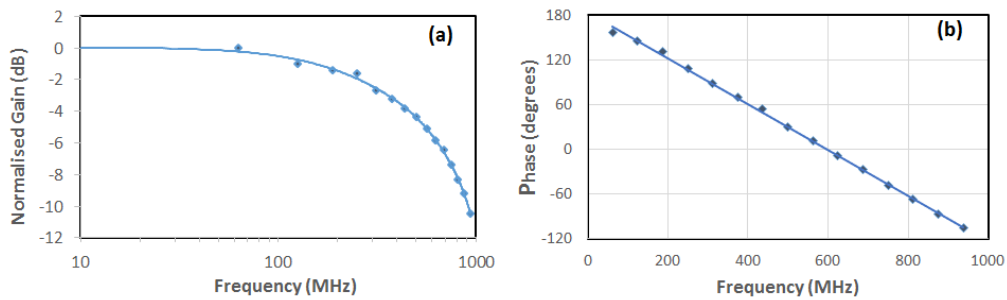


Fig. 6 (a) Normalized amplitude response $|H(f)|$ and (b) Phase response $\angle H(f)$ of the physical point-to-point DFMA-PON system from DAC input to (DSO) ADC output with 26km SSMF included. The response is normalized to the gain at the first subcarrier.

### *5.2 OFDM Subcarrier BER Improvements*

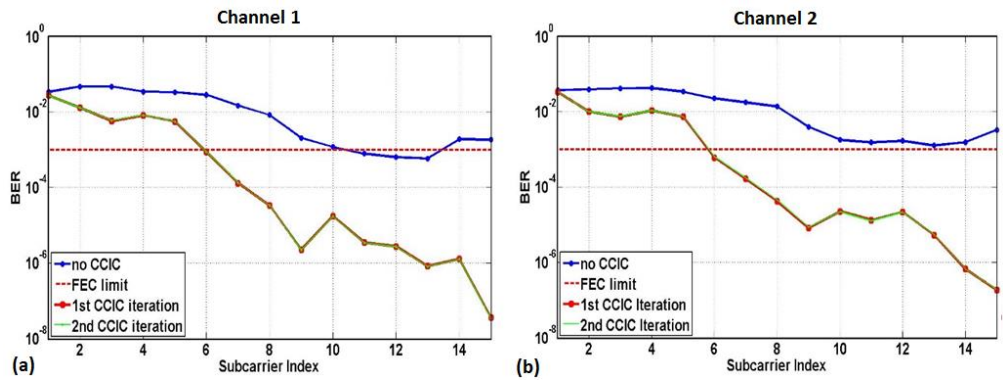


Fig. 7. BER vs. subcarrier index with and without the CCIC technique at a received optical power of -14dBm (a) Channel 1, (b) Channel 2

The improvements in individual OFDM subcarrier BERs due to the CCIC technique are first explored in this subsection. For transmission over 26 km of SMF at a ROP of -14dBm, Fig. 7

shows the BERs for each individual data-carrying OFDM subcarrier for the cases of: i) no CCIC applied, ii) one CCIC iteration applied and iii) two CCIC iterations applied. Fig. 7(a) is plotted for channel 1 (in-phase) and Fig. 7(b) is plotted for channel 2 (quadrature-phase). It is clear in Fig.7 that at the ROP of -14dBm, when the CCIC technique is not applied, very few subcarriers can comply with the adopted FEC limit of $1.0\times10^{-3}$, in fact only 3 subcarriers on channel 1 are only marginally below the FEC requirement. However, when one iteration of the CCIC technique is applied, Fig. 7 shows that the subcarrier BERs are substantially improved and a total of 20 subcarriers (6-15 on each channel) now achieve BER levels below the adopted FEC limit. The total BER for subcarriers 6-15 on channel 1 (channel 2) is now as low as $1\times10^{-4}$ ($6\times10^{-5}$). Also, a single iteration of the CCIC technique achieves a highly notable improvement in BER of more than 1000 times on some individual subcarriers. An important result also shown in Fig. 7 is that the second CCIC iteration does not improve the subcarrier BER performance any further, thus as convergence has been reached further higher order iterations cannot achieve any additional improvements in BER performance. The results therefore indicate that the CCIC technique is powerful enough to only require a single iteration.

It can also be seen in Fig.7 that higher frequency subcarriers of both channels experience greater improvements in BER compared to lower frequency subcarriers. This can be attributed to the fact that the signal spectrum after up-sampling and digital filtering by the shaping filter, consists of two mirrored spectral images having an upper sideband and a lower sideband with subcarrier images mapped to both sidebands. In comparison with the higher frequency subcarriers, the images from the lower frequency subcarriers see greater frequency separations and thus greater amplitude variations at the receiver due to the system frequency response roll-off effect. The removal of the unwanted signal in the receiver relies on the frequency components from each image sideband cancelling out after the down-sampling function, as this maps both images to the same baseband spectral region but with phase differences of 180°, the larger the difference in amplitude of the two frequency components, the weaker the signal cancellation effect is. Lower frequency subcarriers thus suffer from greater CCI and the CCIC technique is less effective at lower frequencies. As such the aforementioned difference occurs.

A very common characteristic of long IMDD links with wide signal spectra is the presence of frequency response nulls in the signal spectral regions. Our work presented in [12], has shown that the CCIC-induced performance gains are not significantly impacted by the nulls because the associated reduction in optical signal-to-noise ratio (OSNR) also plays a significant role in determining the maximum achievable transmission performances.

### *5.3 Capacity versus Reach Improvements*

To explore the maximum improvements in capacity versus reach performance due to the CCIC technique, the following experimental procedures are adopted: without CCIC enabled in a fixed SMF fiber length of 36km, the ROP is reduced until the lowest possible aggregated signal transmission capacity is reached at a BER below $1\times10^{-3}$. At a ROP of -16.6dBm only a single subcarrier on channel 1 can be supported, whilst on channel 2 there does not exist a single subcarrier capable of carrying information. Under these conditions, as 16-QAM modulation is employed, the total net bit rate of is only 0.1Gb/s. With the identified ROP of -16.6dBm and CCIC still disabled, maximum signal transmission capacities are also determined for each channel at different fiber lengths of 26km and 10km. The maximum signal transmission capacities on each channel are then determined for these three fiber lengths with CCIC enabled. In exploring the maximum signal transmission capacities for different fibre lengths with and without the CCIC technique, the receiver RF signal levels are always adjusted for each fibre length to maximize the corresponding signal transmission capacity at a BER below $1\times10^{-3}$ on each subcarrier.

Figure 8(a) shows the net signal transmission capacity versus reach for each channel with and without CCIC enabled. It is shown that without CCIC channel 2 cannot support any data transmission even at a fiber length of 10km, whereas channel 1 can only support two

subcarriers when fiber length is reduced to 10km. However, when CCIC is enabled channel 1 (channel 2) can now support 10 (9) subcarriers, thus giving a net signal transmission capacity of 1 (0.9) Gb/s. The reason why channel 2's performance with and without CCIC is always worse than channel 1 at the adopted ROP is due to the fact that channel 2 is the quadrature-phase channel, whose filter impulse response deviates further from the ideal filter response compared to the channel 1's in-phase filter [7].

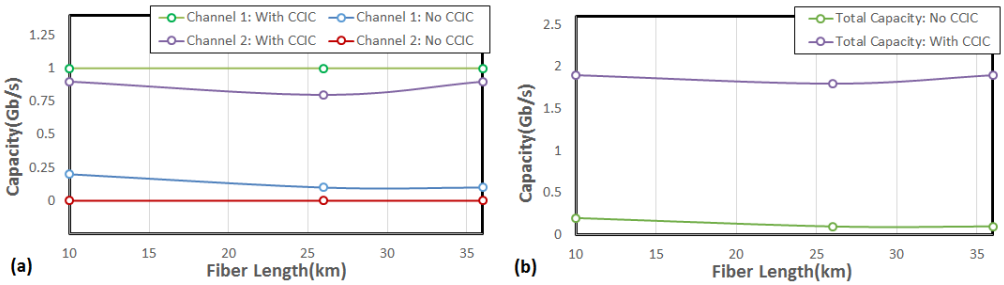


Fig. 8. Capacity vs. reach with and without the CCIC technique at a ROP = -16.6dBm.
(a) Two individual channels (b) Combined channels

Figure 8(b) shows the total aggregated net signal transmission capacity versus reach for both channels combined. Here the total signal transmission capacity can increase from 0.1Gb/s to 1.9Gb/s due to the CCIC technique, thus CCIC achieves an increase in signal transmission capacity as large as 19 times. It is also important to note that Fig. 8 reveals that signal transmission capacities are not dependent on the adopted fiber lengths, this indicates that the DFMA technique preserves the OFDM signal tolerance to the chromatic dispersion effect.

### *5.4 Power Budget Improvements*

Finally, the improvements in power budget due to the CCIC technique are investigated in Fig.9. To provide a suitable CCIC-free reference operating point, for a 36km SMF transmission system, an appropriate adjustment is made to ROP to ensure that the 6 highest frequency subcarriers on each channel are capable of operating at BERs below the adopted FEC limit of $1.0\times10^{-3}$ for the cases of with and without the CCIC technique applied. The aggregated total net signal transmission capacity is 1.2Gb/s (0.6Gb/s per channel). Under these conditions, Fig. 9 shows the BER versus ROP curves for each channel with and without CCIC enabled. It can be seen that both channels exhibit very similar BER developing trends in each case. The power budget improvement can be as large as ~3.5dB for each channel, when the aggregated signal transmission capacity is fixed.

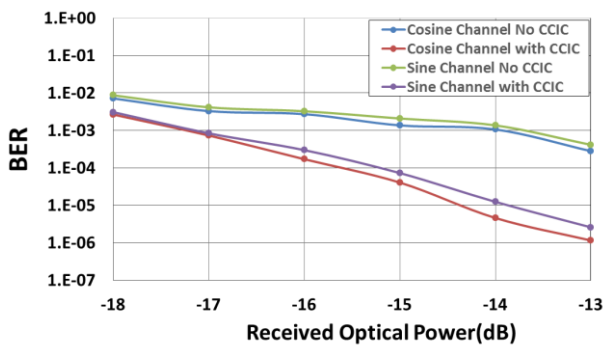


Fig. 9. BER vs. received optical power with and without the CCIC technique over 36km SMF.
Subcarriers 10-15 enabled on each channel.

## 6. Conclusions

The CCI effect between two orthogonal channels sharing the same spectral region can severely degrade the transmission performance in an IMDD-based DFMA PON system. A DSP-based CCIC technique has been experimentally demonstrated which is shown to have relatively low complexity and be highly effective at mitigating the CCI effect for significantly improving the DFMA PON performance. The CCIC technique has the following four unique characteristics; i) the performance rapidly converges after only a single CCIC iteration, ii) the DSP operation is not dependent on the employed modulation formats, iii) the DSP complexity is lower compared to other techniques such as SIC and iv) the performance is not dependent on initial system conditions.

The CCIC technique has been experimentally demonstrated in a two channel point-to-point IMDD DFMA PON system, detailed investigations of the CCIC impact on transmission performance have been undertaken with the following substantial improvements observed: i) reduction in individual subcarrier BERs of over 1000 times, ii) increase in aggregated signal transmission capacity by a factor of 19 times and iii) increase in optical power budget of ~3.5dB. This work demonstrates that the CCIC technique is potentially capable of radically improving the transmission performance in DFMA-PONs. Subsequent research work has investigated the application of a modified CCIC technique in an upstream DFMA-PON with multiple optical network units (ONUs) [12], the modified CCIC technique is also shown to be highly effective for multi-channel DFMA systems.

## Funding

Innovative UK (Project 131816); IRAQI Ministry of Higher Education and Scientific Research (MOHESR).